Journal of Structural Biology 218 (2026) 108327

Contents lists available at ScienceDirect

Journal of Structural Biology

journal homepage: www.elsevier.com/locate/yjsbi

Research Article

Crystal structure, thermostability and temperature-dependent enzymatic activity of an *exo*-β-D-glucosaminidase from *Pyrococcus chitonophagus*

Katarzyna Biniek-Antosiak [a], Daniel Baranowski [a], Joanna Śliwiak [a], Mariusz Milik [b], Magdalena Bejger [a], Wojciech Rypniewski [a,*]

[a] *Institute of Bioorganic Chemistry, Polish Academy of Sciences, Noskowskiego 12-14, 61-704 Poznań, Poland*
[b] *Kraków, Poland*

ARTICLE INFO

Editor Name: Bauke Dijkstra

Keywords:
Exo-β-D-glucosaminidase
Hyperthermophile
Pyrococcus chitonophagus
Crystal structure
Thermodynamics
Enzymatic activity

ABSTRACT

Pch-GlmA is a hyperthermophilic GH35 *exo*-β-D-glucosaminidase whose structure closely resembles its archaeal homologs, yet its functional behavior differs markedly. Calorimetric and fluorimetric temperature scans consistently reveal a complex thermodynamic profile of the enzyme, characterized by distinct thermal transitions. The freshly purified protein appears to be monomeric and required thermal annealing to attain its biologically relevant dimeric state. Catalytic activity is observed only above 75 °C, where the enzyme specifically hydrolyses the glycosidic bond of GlcN–GlcNAc. These findings support a sequential role for *Pch*-GlmA alongside *Pch*-Dac in the processing of chitin-derived carbohydrates. Comparison with related GlmA proteins demonstrates that substantial structural similarity does not necessarily translate into equivalent enzymatic properties and that hyperthermophilic enzymes may operate within narrow temperature ranges. Overall, this work underscores the importance of experimental validation when interpreting or predicting the activity of enzymes derived from extremophiles.

1. Introduction

Chitin is the second most abundant biopolymer after cellulose, with an estimated annual production of 10^{10}–10^{11} tons (Gooday, 1990). It is composed of *N*-acetyl-D-glucosamine (GlcNAc) units linked by β-(1 → 4) glycosidic bonds and stabilized by a dense network of inter-chain hydrogen bonds, which render chitin insoluble in water and highly resistant to degradation. For organisms capable of utilizing it, chitin serves as a rich source of energy and macroelements, including nitrogen—unlike cellulose, which lacks nitrogen. Chitin is metabolized primarily by archaea and bacteria, and to a lesser extent by fungi. Despite its abundance, humans make only limited use of chitin.

Organisms that degrade chitin employ both exo- and endochitinases to cleave the poly-GlcNAc chains into short oligomers, followed by accessory enzymes that process these fragments further. The products of chitinases can be monomerized, deacetylated, deaminated, or phosphorylated. Alternatively, chitin can undergo initial deacetylation to yield chitosan, which can then be hydrolyzed into glucosamine oligomers or monomers.

A distinct mechanism of chitin degradation was discovered in the archaeon *Thermococcus kodakarensis* and later in *Pyrococcus horikoshii*. In this pathway, GlcNAc dimers produced by chitinases are deacetylated and subsequently monomerized by a pair of enzymes: diacetylchitobiose deacetylase (Dac, EC 3.5.1.105) and an *exo*-β-D-glucosaminidase (GlmA, EC 3.2.1.165) (Tanaka et al., 2004; Tanaka et al., 2003). The initial product of Dac, 1,4-β-D-*N*-acetylglucosaminyl-D-glucosamine (GlcN-GlcNAc), is hydrolyzed by GlmA to yield D-glucosamine (GlcN) and GlcNAc; the latter is subsequently deacetylated by Dac (Fig. 1). The end product of this pathway is GlcN, which can be readily metabolized.

The molecular structures, reaction mechanism and substrate specificity of Dac orthologs from *P. horikoshii* and *P. furiosus* (Mine et al., 2014; Nakamura et al., 2016; Nakamura et al., 2015), and more recently from *P. chitonophagus* (Biniek-Antosiak et al., 2022) have been investigated. These studies characterized the enzymes as zinc metalloenzymes that act on the non-reducing end of GlcNAc monomers, dimers or trimers, with the highest activity observed for dimers.

The structure of GlmA, the second enzyme in the "short" chitin-degradation pathway of archaea, has also been reported (Mine and Watanabe, 2019). GlmA appears to be unrelated to the *exo*-β-D-glucosaminidases found in bacteria and eukaryotes. Instead, it belongs to the

* Corresponding author.
E-mail address: wojtekr@ibch.poznan.pl (W. Rypniewski).

https://doi.org/10.1016/j.jsb.2026.108327
Received 20 February 2026; Received in revised form 21 May 2026; Accepted 22 May 2026
Available online 23 May 2026

GH35 family of glycoside hydrolases. Despite its distinct substrate specificity, GlmA shows amino acid sequence homology to segments of β-galactosidases from the GH35 and GH42 families. Although sequence identity is low (15–17%), GlmA shares a similar domain architecture within its subunits with GH42 β-galactosidases, while its active site geometry resembles that of GH35 β-galactosidases. Notably, GlmA is dimeric—like GH35 β-galactosidases—rather than trimeric, as in the GH42 family.

Pyrococcus (formerly *Thermococcus) chitonophagus* is a chitin-degrading, hyperthermophilic, anaerobic archaeon isolated from a deep-sea hydrothermal vent off the west coast of Mexico at a depth of 2600 m (Huber et al., 1995). In a previous study, we analyzed the structure, thermodynamics and substrate specificity of the Dac enzyme from this organism (*Pch*-Dac), which functions upstream of GlmA on the archaeal "simple" chitin-degradation pathway. In the present study, we describe the structure, thermodynamic properties and enzymatic characteristics of the corresponding GlmA enzyme from *P. chitonophagus* (*Pch*-GlmA).

2. Results

2.1. Overall structure

The crystal structure of *Pch*-GlmA was determined at 2.1 Å resolution using synchrotron radiation. The asymmetric unit of the orthorhombic $C222_1$ cell contains a single *Pch*-GlmA subunit and the full unit cell comprises four *Pch*-GlmA dimers generated by crystallographic twofold axes and face-centering operations. Each *Pch*-GlmA subunit (91 kDa) consists of 781 amino acid residues and is organized into three distinct domains: a TIM-barrel domain (residues 1–434), an α/β domain (residues 435–647) and a β domain (residues 648–781) (Fig. 2).

Overall, the structure closely resembles those of homologous GlmA proteins from *T. kodakarensis* (PDB ID: 5GSM), *P. horikoshii* (PDB ID: 5GSL) and *P. furiosus* (PDB ID: 6JOW) (Mine et al., 2017; Mine and Watanabe, 2019; Mine and Watanabe, 2019). Although *Pch*-GlmA shares only 15–29% sequence identity with GH42 β-galactosidases, it retains a similar subunit topology. However, its β-domain features an additional subdomain formed by eight β-strands (4–7 and 4′–7′; Fig. 2a, b).

The *Pch*-GlmA dimer features a central cavity that accommodates the substrate-binding and active sites. The cavity is accessible to solvent via a channel approximately 20 Å in diameter (Fig. 3). Analysis of the crystal structure using PISA (Protein Interfaces, Surfaces, Assemblies) software (Krissinel and Henrick, 2007) further supports a dimeric assembly, with a buried surface area of 14,270 $Å^2$, corresponding to 28% of the total surface area of the dimer (50,920 $Å^2$), and an estimated solvent free energy gain upon complex formation of 112 kcal/mol.

2.2. Substrate-binding site of Pch-GlmA

The binding site of GlmA was previously analyzed by (Mine et al., 2017) in the crystal structure of *T. kodakarensis* enzyme in complex with the reaction product (GlcN), as well as through comparisons with β-galactosidases (Mine and Watanabe, 2019). These studies indicated that GlmA catalyzes hydrolysis of the glycosidic bond between the GlcN and GlcNAc residues via a double-displacement, retaining mechanism. The authors identified the residues functioning as the acid/base catalyst and the nucleophile, along with several residues important for substrate specificity.

In *Pch*-GlmA, the residues forming the substrate binding site closely correspond to those in the *T. kodakarensis* enzyme (PDB ID: 5GSM) (Fig. 4a, b). Glu178 is the likely acid/base catalyst (equivalent to Glu179 in the *T. kodakarensis* structure), whereas Glu346 is the proposed nucleophile (equivalent to Glu347 in the reference structure). An ordered water molecule in the *Pch*-GlmA structure occupies a position equivalent to that of the GlcN amino group in the related complex. The water molecule is coordinated by the hydroxyl group of Tyr52 and the carboxylate groups of Asp177, Glu178 and Glu346. A second ordered water molecule corresponds to the position of the O4 hydroxyl group of GlcN in the *T. kodakarensis* GlmA structure.

2.3. Substrate docking

Molecular docking was performed to explore how the GlcN-GlcNAc substrate might bind to *Pch*-GlmA. The GlcN residue was initially positioned to match the orientation of the GlcN molecule bound to the

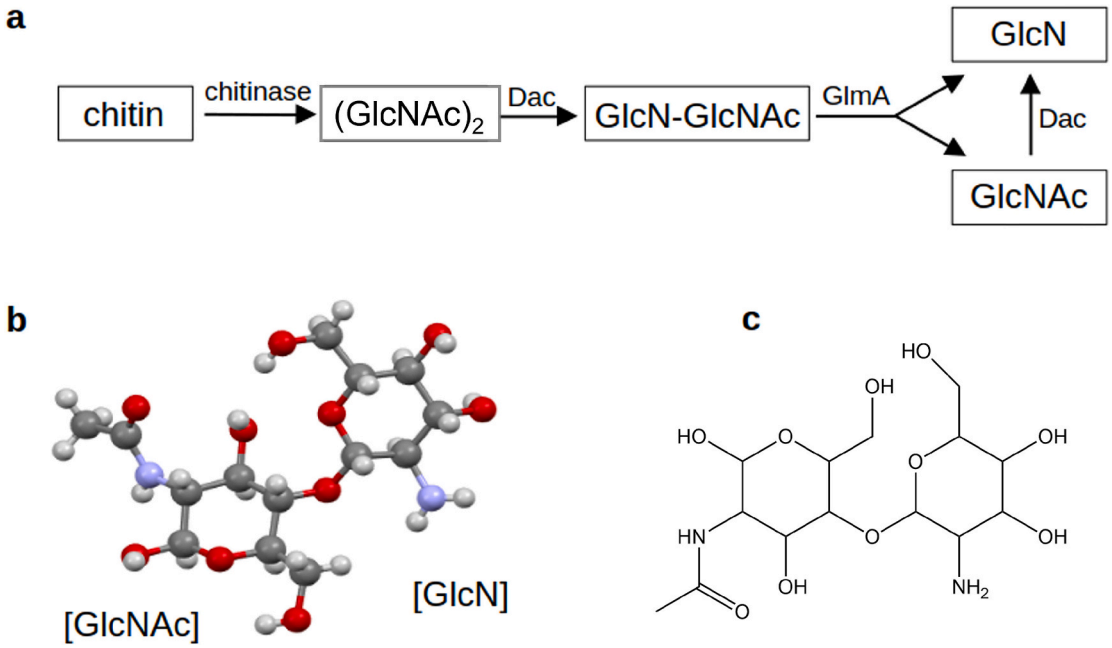

Fig. 1. (**a**) Chitin-degradation pathway discovered in archaea, involving diacetylchitobiose deacetylase (Dac) and *exo*-β-D-glucosaminidase (GlmA) (Tanaka et al., 2004; Tanaka et al., 2003). (**b, c**) Ball-and-stick model and chemical structure of 1,4-β-D-glucosaminyl-D-*N*-acetylglucosamine (GlcN-GlcNAc), the product of Dac and the substrate of GlmA.

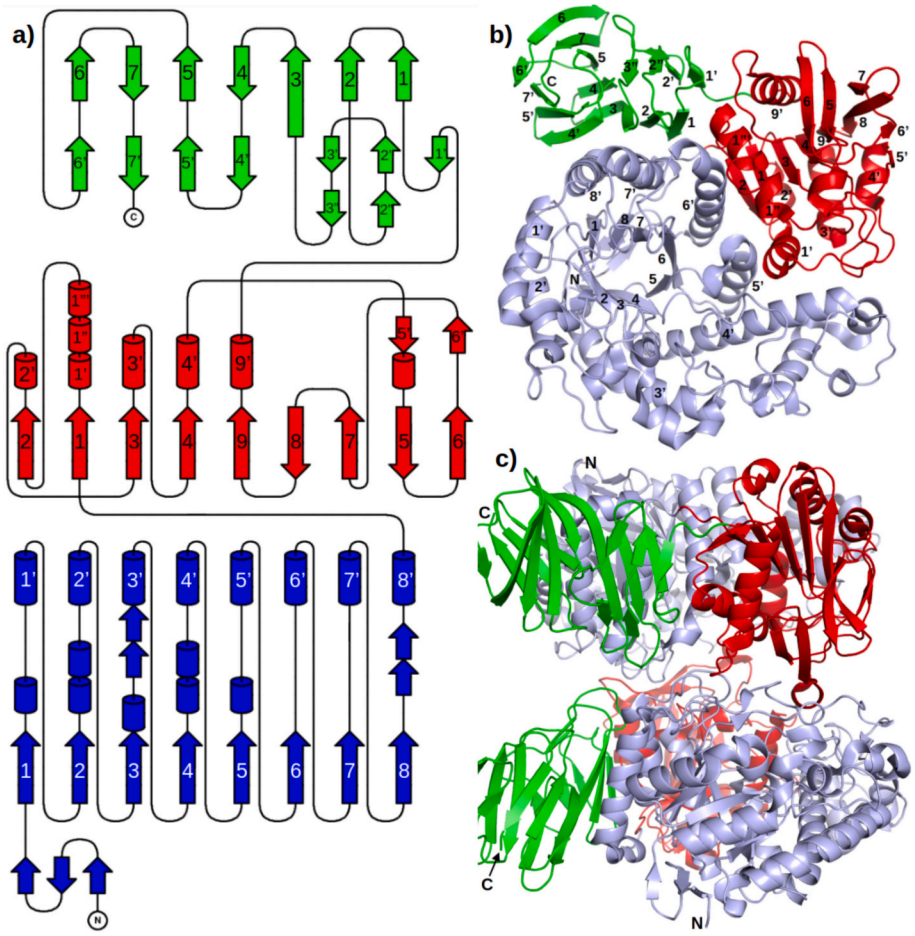

Fig. 2. **a)** Topology diagram of *Pch*-GlmA subunit: the TIM-barrel domain (*blue*), the α/β domain (*red*), and the β domain (*green*). α-helices are shown as cylinders, β-strands as arrows. **b)** Cartoon representation of a *Pch*-GlmA subunit. **c**) Dimer of *Pch*-GlmA subunits as observed in the crystal structure. (For interpretation of the references to colour in this figure legend, the reader is referred to the web version of this article.)

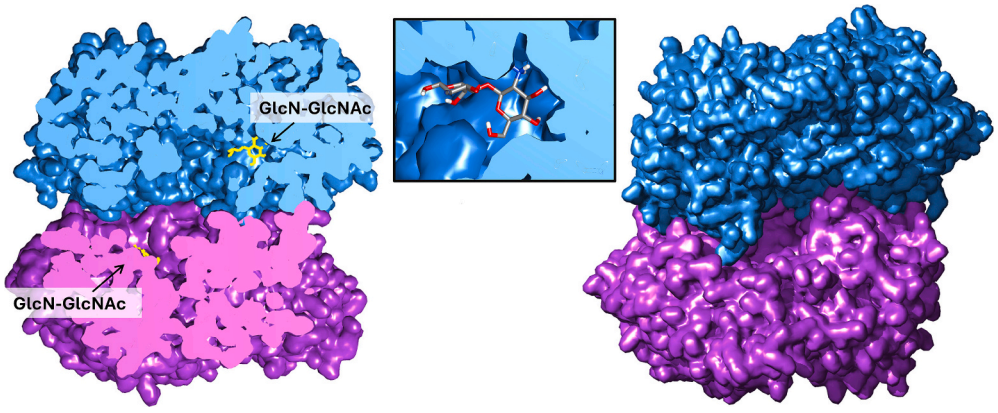

Fig. 3. A surface representation of a *Pch*-GlmA dimer highlights the central cavity that houses the substrate-binding and active sites. The two subunits are shown in *blue* and *violet*. No ligand is present in the crystal structure of *Pch*-GlmA; the GlcN-GlcNAc substrate molecules depicted as sticks were modeled by docking (see the main text for details).

T. kodakarensis GlmA structure (Mine et al., 2017), while the GlcNAc residue was oriented to avoid major steric clashed with the protein.

Subsequent energy optimization and automated adjustment of the substrate and nearby protein residues produced a plausible fit of the ligand within the binding cavity. The resulting model shows a network of hydrogen bonds between the hydroxyl and amino groups of the ligand and the charged or polar residues of the protein (Fig. 4c, d).

The GlcN residue fits into a well-defined cavity within the protein. Three negatively charged residues (Asp177, Glu178 and Glu346) cluster around the positively charged amino group of GlcN. In the *T. kodakarensis* GlmA structure, the residues equivalent to Glu178 and Glu346 have been proposed to function as the acid-base catalyst and the nucleophile, respectively, while the residue corresponding to Asp177 was identified as important for substrate recognition (Mine et al., 2017).

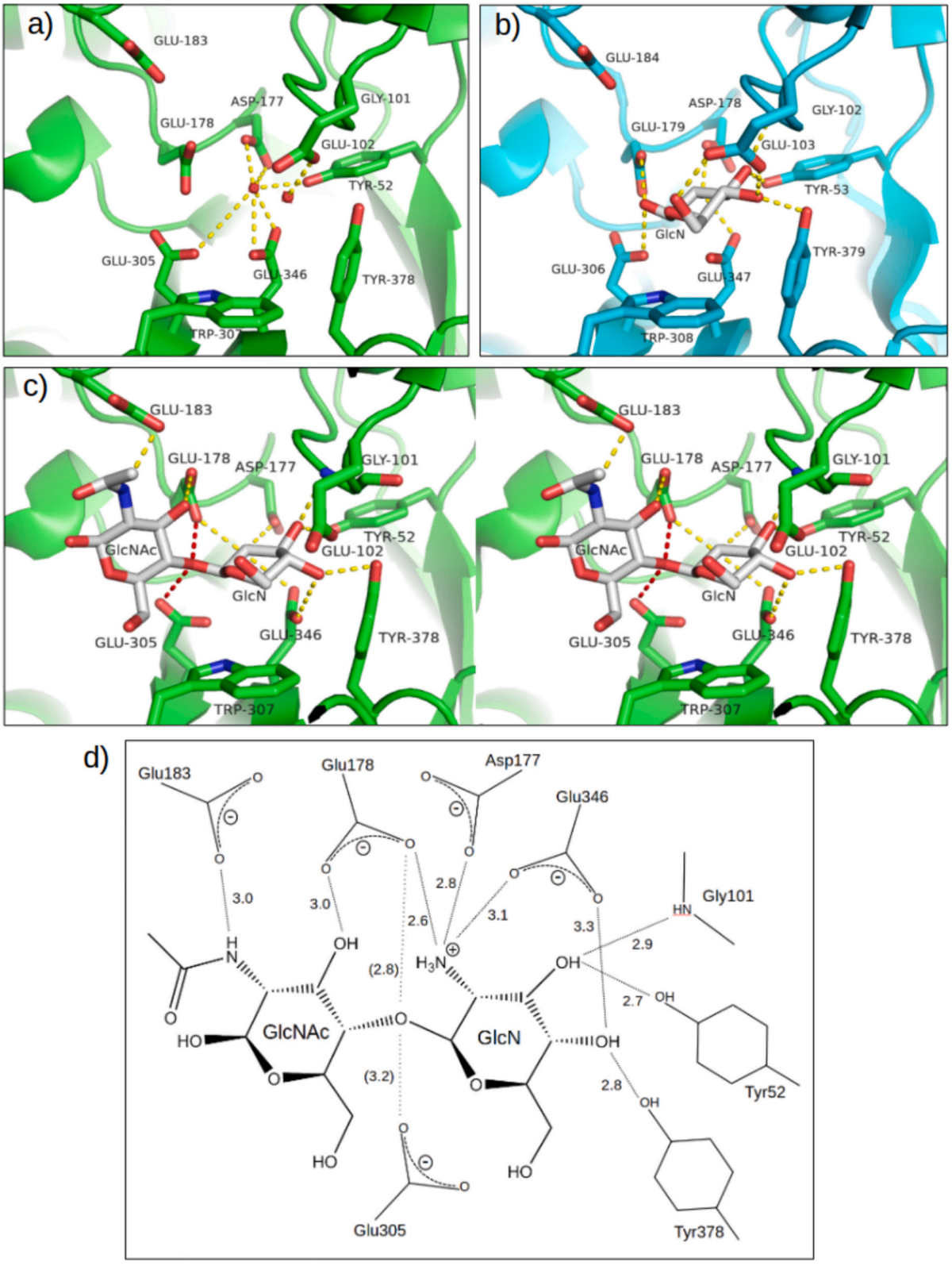

Fig. 4. The active and substrate-binding site in (**a**) *Pch*-GlmA in the absence of ligand, showing only two ordered water molecules (*red* spheres). (**b**) The corresponding site in GlmA from *T. kodakarensis* (PDB code 5GSM) with bound glucosamine (GlcN), the product of the enzymatic reaction. (**c**) Stereo pair showing the result of substrate GlcN-GlcNAc (sticks with *gray* carbon atoms) docking in the active site of *Pch*-GlmA (*green* carbon atoms). Close contacts with the glycosidic oxygen atom are marked in *red*. (**d**) Schematic representation of the hydrogen-bonding network between the docked substrate and *Pch*-GlmA. Distances are given in Å. Values in parentheses indicate the distances from the glycosidic oxygen atom to Glu178 and Glu305. (For interpretation of the references to colour in this figure legend, the reader is referred to the web version of this article.)

In contrast, the GlcNAc residue occupies a more open region of the binding cavity than GlcN. It forms only two hydrogen bonds with the protein that may contribute to substrate binding: one between the hydroxyl group at position 3 and the catalytic Glu178, and another between its amino group and Glu183.

The glycosidic oxygen atom makes close contacts with Glu178, proposed as the acid/base catalyst, and with Glu305, whose equivalents in related GlmA enzymes have been shown to enhance catalytic activity (Mine et al., 2017).

2.4. Thermal stability and melting profile of Pch-GlmA

Differential scanning calorimetry (DSC) revealed that *Pch*-GlmA is a highly thermally stable protein. It exhibits a complex melting profile that appears to be independent of protein concentration (data not shown). Four distinct thermal transitions were identified at 73 °C, 92 °C, 106 °C and 111 °C based on fitting of the raw DSC data (Fig. 5).

The experimental results are not straightforward to interpret; however, the lowest-temperature transition at 73 °C can be attributed to dimerization of protein subunits (see DSF/DLS results below). The higher-temperature peaks likely correspond to thermal unfolding of the protein, followed by aggregation (see DLS results below).

Further studies of *Pch*-GlmA stability in solution were carried out using nano-Differential Scanning Fluorimetry (nanoDSF). The accessible temperature range of the nanoDSF instrument enabled thermal scanning from 25 to 105 °C. This analysis confirmed two thermal transitions previously identified by DSC, occurring at 73.1 ± 1.1 °C and 91.7 ± 0.1 °C, respectively (Fig. 6, blue trace). Analysis of the cumulant hydrodynamic radius as a function of temperature revealed a marked increase in particle size coinciding with the first transition, around 73 °C.

Based on this observation, the experiment was repeated using a heat-treated sample. Heating the protein at 73 °C for 25 min induced a permanent change in its oligomeric state upon cooling, accompanied by an increase in the hydrodynamic radius from 10.14 ± 0.01 nm to 18.88 ± 0.01 nm (Fig. 6, lower panel). Notably, both samples exhibited low polydispersity indices (PDI; 0.18 ± 0.01 and 0.11 ± 0.02, respectively), indicating high sample homogeneity.

Furthermore, the temperature scan of the heat-treated sample (Fig. 6, pink trace) demonstrated the absence of the thermal transition at ~73 °C, while the second transition persisted and was slightly shifted to a higher temperature (92.2 ± 0.4 °C). Importantly, the hydrodynamic radius of the heat-treated sample remained constant up to the transition at ~92 °C.

2.5. Enzymatic tests by isothermal titration calorimetry (ITC)

Four potential substrates were tested: $(GlcNAc)_2$, $(GlcN)_2$, GlcN–GlcNAc and GlcNAc–GlcN, as well as 4-nitrophenyl-*N*-acetyl-β-D-glucosaminide, an artificial substrate. Enzymatic assays were conducted between 25 and 75 °C. Within the tested temperature range, the results were inconclusive: the apparent enthalpy ("H_{app}") values varied from −100 to −300 cal/mol, far too small to reflect covalent bond cleavage. NMR spectroscopy confirmed that no reaction occurred under these conditions (see below).

Additional enzymatic tests were therefore performed by incubating the enzyme with the potential substrates at higher temperatures (90 °C), with reaction products assessed exclusively by NMR spectroscopy (see below).

2.6. Identifying the reaction products by NMR spectroscopy

Preliminary ^{1}H and ^{13}C NMR measurements were recorded for *Pch*-GlmA following incubation at 60 °C for 1 h with GlcN–GlcNAc, GlcNAc–GlcN and 4-nitrophenyl-*N*-acetyl-β-D-glucosaminide (Fig. S1–S5, S8). No changes in chemical shifts were observed relative to the reference spectra, corroborating the ITC data and indicating the absence of detectable enzymatic activity under these conditions. Consequently, all subsequent NMR experiments were performed using samples incubated at 90 °C.

Analysis of the ^{1}H and ^{13}C NMR spectra of chitobiose $(GlcN)_2$ and its monoacetylated (GlcNAc–GlcN, GlcN–GlcNAc) and diacetylated $(GlcNAc)_2$ derivatives in HEPES/D_2O following incubation with *Pch*-GlmA at 90 °C revealed the presence of both substrate and product in the case of GlcN–GlcNAc (Figs. 7–8, S3–S5). In contrast, the ^{1}H NMR spectra of the other three compounds remained unchanged (Fig. S1–S2, S6–S7), clearly indicating that *Pch*-GlmA is inactive toward these compounds and exhibits specificity for GlcN–GlcNAc.

The reducing end of chitobiose and its acetyl derivatives undergoes anomerization at C1', resulting in complex ^{1}H and ^{13}C NMR spectra for both the post-reaction mixtures and reference samples. As a result, reliable monitoring of reaction progress using 1D NMR was limited to narrow spectral regions corresponding to the anomeric proton/carbon (H1'/C1') and the amide NH signal (Figs. 7–8 and S1–S5). However, additional reliable assignments of ^{1}H and ^{13}C signals were obtained from the comparative analysis of 2D spectra, i.e. COSY and ^{1}H—^{13}C HSQC type spectra, which allowed an approximate estimation of the composition of the post-reaction samples as well as reference samples (Fig. S9–S21). The 1D and 2D spectra for GlcN–GlcNAc, GlcNAc and

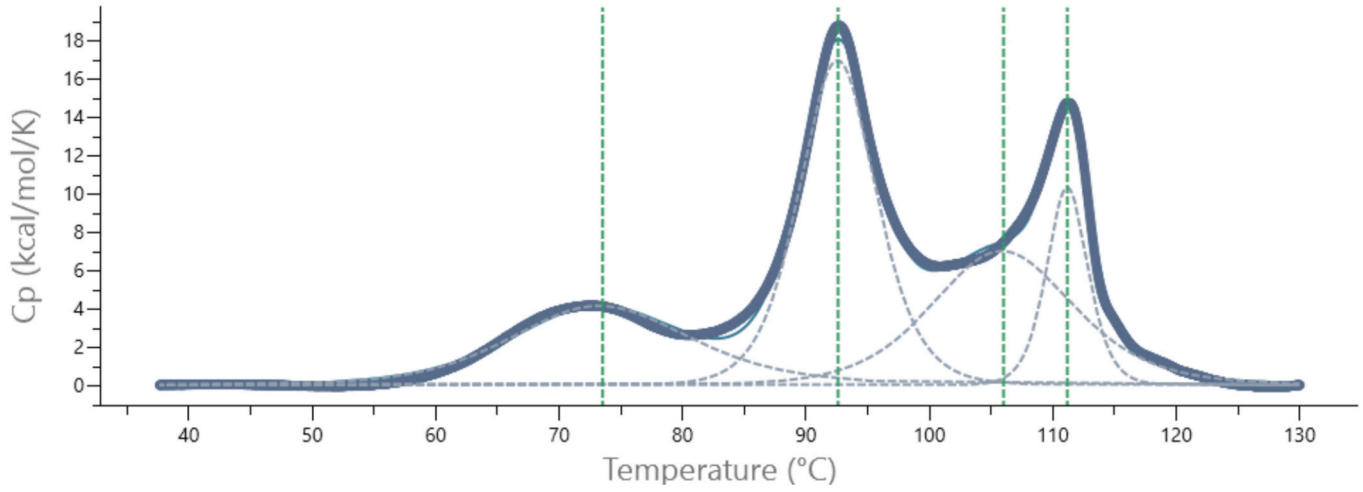

Fig. 5. DSC heating-scan profile of *Pch*-GlmA. The solid line shows the overall melting profile, while the dotted lines show the possible interpretations of the experimental curve in terms of underlying Gaussian-like individual thermal events.

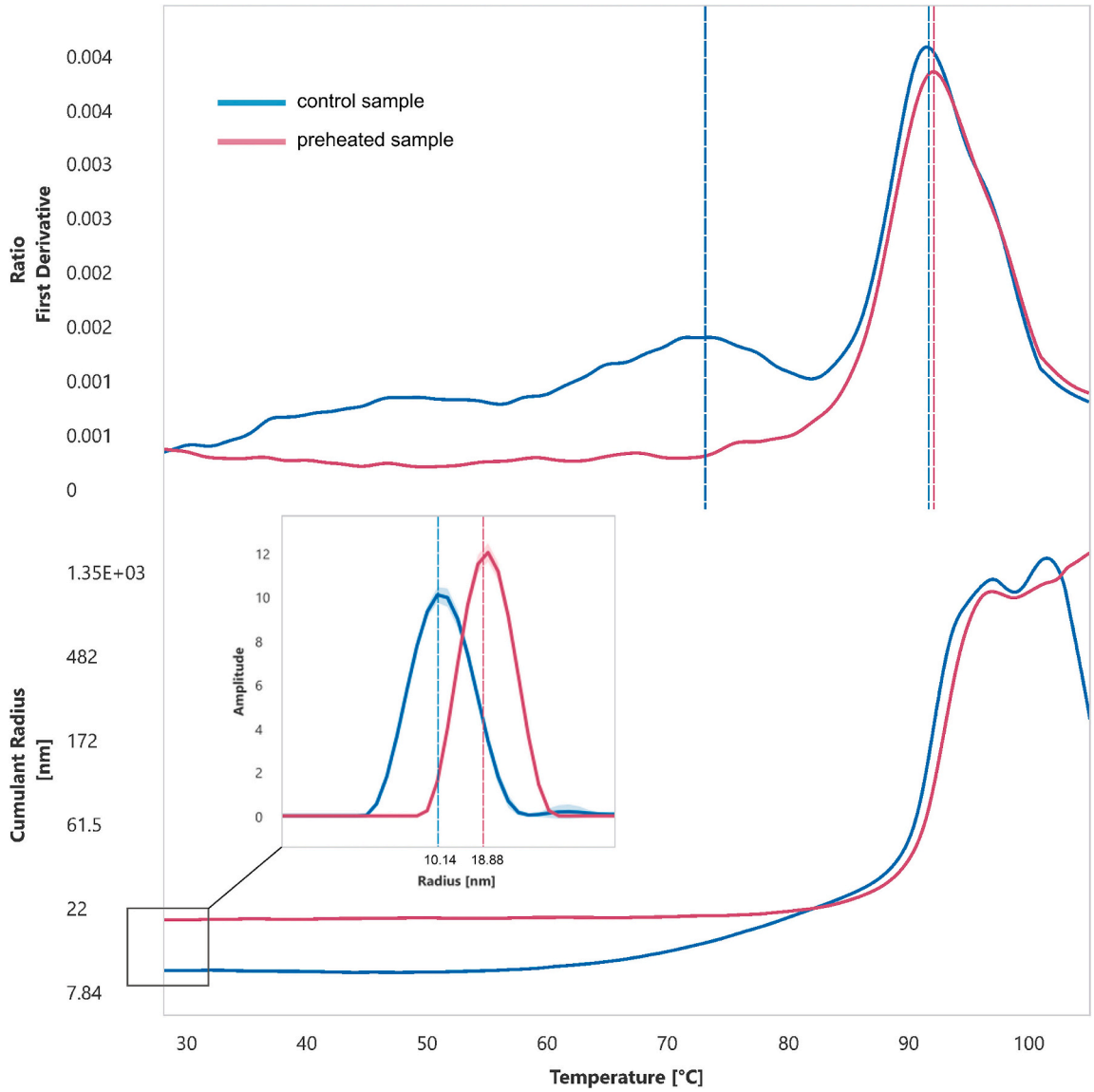

Fig. 6. Melting curves (upper panel) and hydrodynamic cumulant radius (lower panel) of *Pch*-GlmA recorded by NanoDSF for non-heated (*blue*) and pre-heated at 73 °C (*pink*) samples. The inset shows a detailed DLS size analysis performed at 25 °C, illustrating the size distribution of both heated and non-heated samples. (For interpretation of the references to colour in this figure legend, the reader is referred to the web version of this article.)

GlcN are presented, together with ^{1}H and ^{13}C signal assignments in Supplementary Figures.

In the ^{1}H NMR spectrum of GlcN–GlcNAc after reaction with *Pch*-GlmA, a new doublet at 5.271 ppm appeared, corresponding to H1' of D-glucosamine (GlcN, denoted as H1'B; Fig. 7F). In addition, the signal at 5.092 ppm broadened due to overlap of the doublets corresponding to H1' of GlcNAc and H1' of GlcN–GlcNAc (denoted as H1'A, respectively; Fig. 7E). These H1' signals represent the major anomeric forms of the analyzed compounds. The chemical shifts of the H1' signals of the minor anomeric form are suppressed due to proximity to the H_2O signal but are visible in the ^{1}H—^{13}C HSQC spectra (Fig. S11). Two doublets corresponding to the amide protons of the major and minor anomers of GlcNAc and GlcN–GlcNAc in the 7.9–8.2 ppm region also shifted upfield by 0.06 ppm, further indicating the predominance of GlcNAc over GlcN–GlcNAc. (Fig. 7A–D).

Analysis of the ^{13}C NMR spectra provided complementary evidence. In the anomeric region (90–105 ppm), two new strong signals at 94.99 and 90.88 ppm appeared in the post-reaction sample, corresponding to the C1' resonances of both GlcNAc anomers, while the C1' signal of the non-reducing end of GlcN–GlcNAc disappeared (Figs. S5 and S10). Furthermore, the 80–45 ppm region of the ^{13}C spectrum of GlcN–GlcNAc exhibited substantially greater complexity than the corresponding spectra of GlcNAc and GlcN, unequivocally demonstrating the predominance of reaction products over the remaining substrate.

3. Discussion

The structural and enzymatic analyses position *Pch*-GlmA within the GH35 family, rather than the related GH42 family (Mine et al., 2017). Recent classifications have distinguished GH35 enzymes from GH42 and have recognized them as also involved in chitin degradation. *Pch*-GlmA represents the fourth described structure of *exo*-β-D-glucosaminidase. Notably, all known GlmA proteins, including *Pch*-GlmA, originate from hyperthermophilic archaea.

The structure of *Pch*-GlmA is similar to those of homologous enzymes from *P. furiosus*, *P. horikoshii* and *T. kodakarensis* (PDB IDs: 6JOW, 5GSL and 5GSM, respectively). This similarity is unsurprising, given their relatively high amino acid sequence identity with *Pch*-GlmA (63–75%), with only a few insertions or deletions (Fig. S23). The amino acid residues responsible for catalysis and those that bind the GlcN residue at the

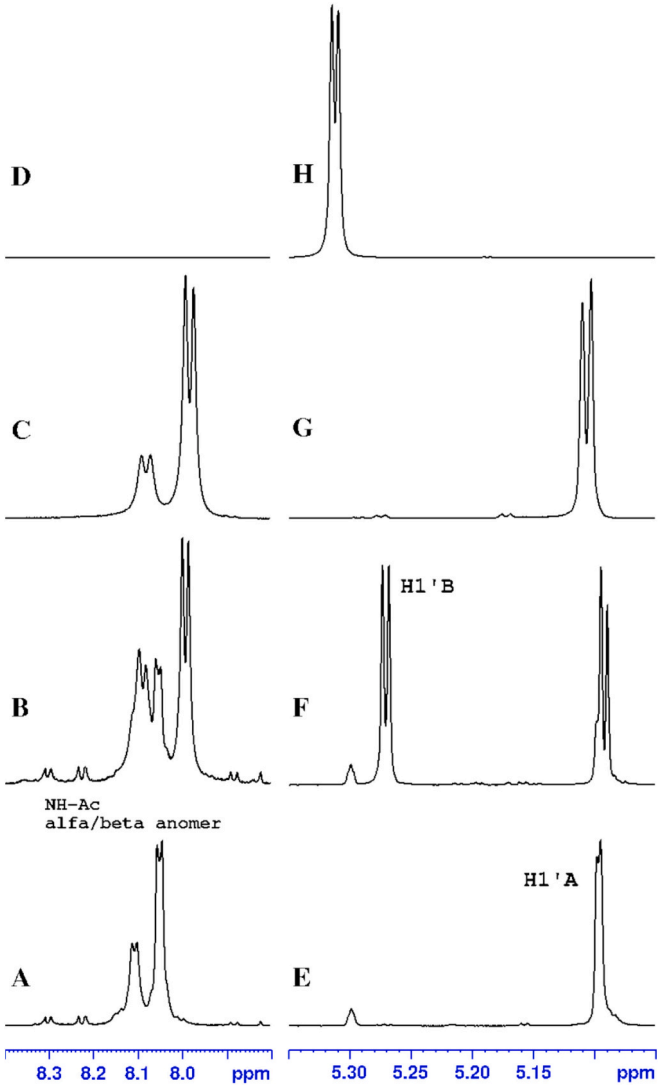

Fig. 7. Representative ^{1}H NMR spectra in the amide region (**A-D**) and anomeric region (**E–H**) for: reference GlcN–GlcNAc (**A**, **E**); GlcN-GlcNAc incubated at 90 °C with *Pch*-GlmA (**B**, **F**); reference GlcNAc (**C**, **G**); and reference GlcN (**D**, **H**). H1'A denotes the anomeric proton of the major form at the reducing end of GlcN–GlcNAc or GlcNAc. H1'B denotes the anomeric proton of the major form of GlcN.

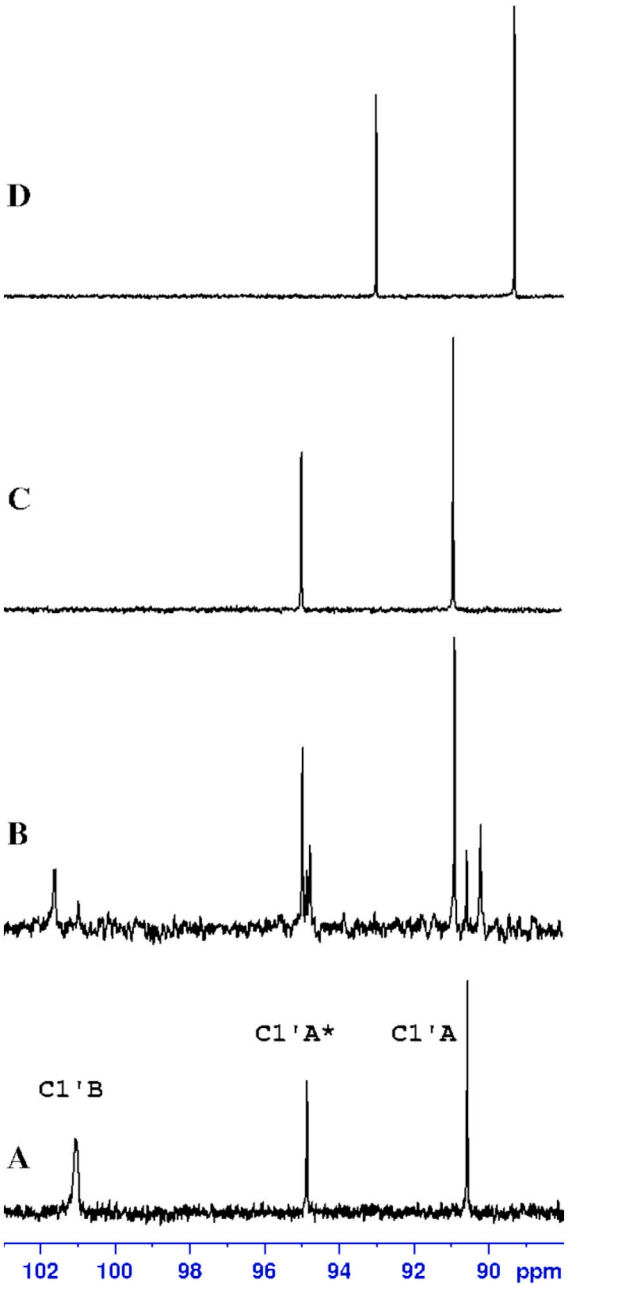

Fig. 8. Representative ^{13}C NMR spectra in the anomeric region for reference GlcN–GlcNAc (**A**); GlcN–GlcNAc incubated at 90 °C with *Pch*-GlmA (**B**); reference GlcNAc (**C**); and reference GlcN (**D**). C1'A and C1'A* denote the anomeric carbons of the major and minor form, respectively, at the reducing end of GlcN–GlcNAc or GlcNAc. C1'B denotes the anomeric carbon at the non-reducing end of GlcN–GlcNAc.

non-reducing end of the substrate have been identified in the related GlmA structure from *T. kodakarensis* (Mine et al., 2017). These key residues are also conserved in *Pch*-GlmA (Fig. 4). However, the binding of the GlcNAc residue at the reducing end of the substrate remains undefined.

A substrate-enzyme complex is unlikely to be captured in a crystal structure because of its transient nature, whereas a theoretical model cannot provide definitive conclusions. Therefore, the molecular docking results for the GlcN-GlcNAc substrate in the *Pch*-GlmA binding site should be regarded as a preliminary sketch of the substrate-enzyme interaction (Fig. 4).

In the model, the GlcN residue interacts with the protein in a manner similar to that observed in the GlcN-bound crystal structure of GlmA from *T. kodakarensis*. The amino group of GlcN is positioned within a cluster of acidic side chains, including the catalytic acid-base residue (Glu178) and the nucleophile (Glu346). This arrangements accounts for the binding site's specificity for a free amino group rather than an *N*-acetyl group at the non-reducing end of the substrate. Furthermore, electrostatic interactions between these catalytic residues with the positively charged amino group likely enhance their polarization, thereby priming them for catalysis. Thus, the substrate itself may contribute to its own degradation.

In contrast to the tightly packed, hydrogen-bonding-rich environment surrounding the GlcN residue at the non-reducing end of the substrate, the region accommodating the sugar on the reducing side is considerably more open. Docking simulations resulted in only two hydrogen bonds, one involving the sugar ring and the other the amino group. The acetyl group of the docked GlcNAc residue does not engage in any close interactions with the protein.

Consequently, this model does not account for the enzyme's selectivity for GlcN-GlcNAc over GlcN-GlcN. It is possible that the substrate

adopts a distinct conformation upon binding. Carbohydrate hydrolysis frequently involves distortion of the glycosidic bond into a high-energy, preorganized geometry prior to cleavage. Such conformational changes may be difficult to capture in silico, as it would appear energetically unfavorable or structurally implausible in static docking models.

Differential scanning calorimetry (DSC) reveals a complex thermodynamic profile of *Pch*-GlmA, with multiple thermal transitions occurring between 65 and 125 °C (Fig. 5). These data are consistent with nanoDSF measurements (Fig. 6).

The first thermal transition, characterized by a peak at 73 °C, is attributable to a pronounced change in the protein's oligomeric state. The initial hydrodynamic radius in solution (~10 nm) increases to approximately 18 nm as the temperature surpasses this transition. Upon cooling, the radius remains at 18 nm, and the 73 °C peak is absent in a subsequent DSF scan. Both the 10 nm and 18 nm species display a high degree of monodispersity, as indicated by DLS signal (Fig. 6). The 18 nm species remains stable up to ~90 °C, after which rapid aggregation is observed.

The protein's initial state (subunit molecular mass 91 kDa) is most likely monomeric, as indicated by its elution profile on a Sephacryl S-100 size-exclusion column (Fig. S24). Although a hydrodynamic radius of 10 nm appears relatively large for a globular protein of this size, deviations from a compact spherical shape or increased conformational flexibility could result in an enlarged effective radius.

In summary, the freshly purified protein appears to be monomeric and requires thermal annealing to attain its biologically relevant dimeric state. Nevertheless, it crystallizes as a dimer, even though crystallization was performed at room temperature. In this case, dimerization may be facilitated by prolonged incubation at high protein concentrations in the crystallization medium.

Enzymatic activity is observed exclusively at temperatures where the protein exists as a dimer. However, the necessity of dimerization for activity remains unclear, given that the substrate-binding site resides within a single subunit. The dimer's structure merely indicates that the entrance to the cavity formed during dimerization may restrict access for ligands larger than approximately 20 Å in diameter to the substrate-binding sites located within the cavity (Fig. 3).

The additional peaks observed at 92, 106 and 111 °C in the DSC thermogram most likely correspond to successive unfolding and aggregation events. The 92 °C transition falls within the operational range of the nanoDSF instrument and is clearly detected in the nanoDSF profile. Notably, this transition coincides with the onset of aggregation, as indicated by the DLS signal (Fig. 6).

These individual peaks may reflect distinct unfolding steps within the subunits, suggesting that different domains of *Pch*-GlmA possess varying thermal stabilities. The stability of TIM-barrel proteins has been investigated in several systems and is characterized by a complex thermodynamic landscape with multiple folding intermediates (Gu et al., 2007).

Enzymatic assays performed at temperatures up to 75 °C revealed no detectable activity of *Pch*-GlmA. Although microcalorimetry may yield an apparent enthalpy change that is too small to detect—owing, for example to compensation between bond cleavage and buffer-related heat effects—NMR analysis independently confirmed that the substrates did not undergo the expected transformation at these temperatures. In contrast, NMR assays of experiments performed at 90 °C demonstrated clear activity and specificity toward GlcN–GlcNAc, the product generated by *Pch*-Dac.

The observed substrate specificity suggests that *Pch*-GlmA may function in tandem with *Pch*-Dac, as proposed for related enzymes (Tanaka et al., 2004). In this model, *Pch*-Dac first deacetylates GlcNAc-GlcNAc at the non-reducing end, after which *Pch*-GlmA cleaves the resulting GlcN-GlcNAc into GlcN and GlcNAc. The remaining GlcNAc is then deacetylated by *Pch*-Dac, yielding GlcN as the final product.

The activity profile of *Pch*-GlmA should be considered in relation to previous enzymatic studies of homologous GlmA proteins. GlmA from *T. kodakarensis* was tested against GlcNAc-GlcNAc, GlcN-GlcN, longer oligomers up to $(GlcN)_6$, and several disaccharides (Tanaka et al., 2003). Activity was observed toward GlcN-GlcN and longer GlcN oligomers. These assays were conducted across a temperature range of 37–100 °C, with an optimum at 80 °C, although activity was detectable at all tested temperatures. Another study reported activity of GlmAs from *T. kodakarensis* and *P. horikoshii* toward GlcN-GlcNAc at 37 °C (Mine et al., 2017).

These findings contrast with those for *Pch*-GlmA, which displays no activity toward GlcN-GlcN and no detectable activity at temperatures up to 75 °C.

The authors were initially puzzled by the lack of *Pch*-GlmA activity under conditions in which the related enzyme *Pch*-Dac displayed clear activity (Biniek-Antosiak et al., 2022). *Pch*-Dac required a pre-incubation (annealing) step at 60 °C, after which measurable activity was observed starting at 25 °C and increasing progressively up to the highest tested temperate of 75 °C. Nevertheless, inactivity of *Pch*-GlmA, or any enzyme, outside its natural operating conditions should not be surprising. The present study demonstrates that enzymes derived from (hyper)thermophilic organisms may be poorly suited to use at temperatures to which they are not evolutionarily adapted and should not be viewed simply as more robust counterparts of mesophilic enzymes.

Moreover, comparison of the structures and activities of *Pch*-GlmA with those of related enzymes indicates that even highly similar proteins can exhibit different functional properties. This underscores the limitations of relying exclusively on homology-based functional predictions.

4. Materials and methods

4.1. Gene cloning, expression and protein purification

Genomic DNA was kindly provided by Prof. Constantinos E. Vorgias (National and Kapodistrian University of Athens). The *Pyrococcus chitonophagus* DSM 10152 *(*formerly *Thermococcus chitonophagus)* gene *chiton_1401* (GenBank code: CUX78180) was inserted into the T7 expression vector pET151D-TOPO, which includes as N-terminal tag codons for 6xHis and a TEV protease cleavage site. The construct was verified by sequencing (Genomed S.A., Warsaw, Poland).

The gene was expressed in BL21-Magic *E. coli* cells in LB medium supplemented with 100 μg/mL ampicillin and 25 μg/mL kanamycin. Gene expression was induced with 0.5 mM IPTG and carried out for 16 h at 18 °C. Cells were harvested by centrifugation and stored at −80 °C until use.

For lysis, the cells were resuspended in buffer containing 50 mM Tris (pH 8.5), 300 mM NaCl, 30 mM imidazole, 10% (*v*/v) glycerol, 0.5% (v/v) Triton X-100 and 1 mM PMSF, then sonicated for a total of 4.5 min. The lysate was clarified by centrifugation at 16,000 rpm for 30 min at 4 °C. The supernatant was applied to a His-bind affinity column (Ni resin) and eluted with 200 mM imidazole in 50 mM Tris (pH 8.5) and 300 mM NaCl (Buffer A). The eluate was placed in a dialysis bag and TEV protease was added at a ratio of 1 mg TEV per 10 mg protein.

A two-step dialysis was performed against Buffer A supplemented with 5 mM 2-mercaptoethanol for a total of 20 h at 4 °C to remove imidazole and cleave the His-tag. The sample was then reapplied to the Ni column to remove any protein that retained the His-tag. The flow-through containing tag-free *Pch*-GlmA was loaded onto a HiPrep 16/60 Sephacryl S-100 column pre-equilibrated with 25 mM Tris (pH 8.5) and 50 mM NaCl, using an ÄKTA chromatographic system. Fractions containing purified *Pch*-GlmA were pooled and concentrated to 12 mg/mL for crystallization (Fig. S24)

4.2. Protein crystallization, data collection, processing, structure solution and refinement

Crystallization was performed using a Gryphon crystallization robot (ARI, Sunnyvale CA, USA). *Pch*-GlmA crystallized in space group $C222_1$

from a solution containing 25% (v/v) PEG 1500 and 0.1 M SPG buffer (succinic acid, sodium phosphate monobasic monohydrate, and glycine; Molecular Dimensions, Rotherham, UK), pH 8.0, at 18 °C. Synchrotron X-ray diffraction data were collected at 100 K on beamline P13, operated by EMBL Hamburg at the PETRA III storage ring (DESY, Hamburg, Germany) (Cianci et al., 2017). Before flash-cooling, crystals were immersed in a cryoprotectant solution prepared by supplementing the reservoir solution with ethylene glycol to a final concentration of 25% (v/v).

X-ray diffraction data were processed using XDS (Kabsch, 2010), and the data are summarized in the Table 1. The structure was solved by molecular replacement with Phaser (McCoy et al., 2007) from the CCP4 suite (Winn et al., 2011), using the glycoside hydrolase A structure (PDB entry 5GSL) as the search model (Mine et al., 2017). Model building was conducted in Coot (Emsley et al., 2010), and refinement was carried out with Refmac5 (Murshudov et al., 2011).

4.3. Modeling protein-ligand interactions

Protein-ligand minimization was performed using UCSF Chimera software, version 1.18 (Pettersen et al., 2004). A model of GlcN-GlcNAc, representing the substrate, was placed in the enzyme's binding site, with the GlcN residue positioned according to the crystal structure of GlmA from *T. kodakarensis*, which contains bound GlcN (Mine and Watanabe, 2019) (PDB ID: 5GSM). The GlcNAc residue was initially oriented manually in Coot (Emsley et al., 2010) to avoid major steric clashes.

A zone was then defined in Chimera that included the preliminarily docked ligand and all atoms and bonds of any protein residue with at least one atom within 5 Å of any ligand atom. Hydrogen atoms were added to the selected atoms, taking into account potential hydrogen bonds. Charges were assigned using the AMBER ff14SB force field (Tian et al., 2020) for standard residues and the semi-empirical AM1-BCC method (Jakalian et al., 2000) for the ligand and any non-standard residues.

Energy minimization of the selected atoms was carried out using Chimera's "Minimize Structure" tool with the following parameters: 1000 steepest descent steps (step size 0.02 Å), followed by 100 conjugate-gradient steps (step size: 0.02 Å). All unselected atoms were kept fixed. These settings were chosen to balance computational efficiency with sufficient structural refinement. The minimization was then repeated on the pre-minimized complex with the selection radius increased to 7.5 Å, allowing a larger portion of the protein to relax.

The pK_a of GlcN–GlcNAc was calculated from the atomic coordinates of the minimized protein–substrate complex using MarvinSketch (Cherinka et al., 2019).

Table 1
Summary of the X-ray data and the final model of *Pch*-GlmA.

PDB code	8OUG
Raw diffraction images DOI	10.60884/YPNUCE
Space group	$C222_1$
Unit cell parameters:	
a (Å)	89.4
b (Å)	120.5
c (Å)	145.6
Wavelength (Å)	0.9763
Resolution (Å)	2.1
R_{merge} [#]	0.111 (1.66)[*]
Completeness (%)	99.6
Observed reflections	612,215
Unique reflections	44,994
<I/σ(I)>	19.4 (2.1)
Protein subunits/asymmetric unit	1
$R^{\S}/R_{free}$ [$]	0.165/0.219

[*] Values in brackets are for the highest resolution shell.

[#] $R_{merge} = \Sigma_{hkl}\Sigma_i|I_i(hkl) - < I(hkl) > |/ \Sigma_{hkl}\Sigma_i I_i(hkl)$, where $I_i(hkl)$ is the integrated intensity of a given reflection and $< I(hkl) >$ is the mean intensity of multiple corresponding symmetry-related reflections.

[§] $R = \Sigma_{hkl}||F_{obs}|-|F_{calc}||/ \Sigma_{hkl} |F_{obs}|$, where F_{obs} and F_{calc} are the observed and calculated structure factors, respectively.

[$] R_{free} is R calculated using a randomly chosen subset of reflections excluded from the refinement.

4.4. Differential scanning calorimetry

The thermal stability of *Pch*-GlmA was evaluated using a MicroCal PEAQ-DSC system (Malvern Instruments Ltd., Malvern, UK). Prior to differential scanning calorimetry (DSC) experiments, the protein sample was dialyzed against the specified buffer (25 mM HEPES, pH 8.0, 200 mM NaCl), which was subsequently used for all DSC measurements.

A standard DSC experiment consisted of two measurements performed under identical instrument conditions: (a) five reference scans with buffer-filled cells to establish the instrument's thermal history and ensure baseline repeatability, and (b) a single sample–buffer scan to obtain melting temperature data for analysis.

Thermal unfolding of *Pch*-GlmA was monitored over a temperature range of 2–130 °C at a scan rate 60 °C/h, using high feedback mode. The protein concentration, determined by NanoDrop spectrophotometry, was 12 mg/mL (134 μM). Additional preliminary experiments were also performed using different experimental settings.

4.5. Nano differential scanning fluorimetry (nanoDSF)

Thermal stability and hydrodynamic radius (derived from the DLS signal) of *Pch*-GlmA were assessed using nanoDSF on a Prometheus NT.48 instrument (NanoTemper Technologies). *Pch*-GlmA, purified by size-exclusion chromatography (SEC) at a concentration of 0.8 mg/mL (determined by absorbance at 280 nm), was heated at 73 °C for 25 min and subsequently centrifuged at 13,000 rpm for 3 min prior to analysis. A non-heated sample served as a control. Detailed DLS size analysis of both samples was performed at 25 °C with the DLS laser power set to 100%. Thermal unfolding was monitored by recording fluorescence emission at 330 and 350 nm during a temperature ramp from 25 °C to 105 °C at a rate of 60 °C/h, with the laser power set to 21%. All measurements were performed in triplicate in SEC buffer (50 mM NaCl, 25 mM HEPES, pH 7.5).

4.6. Microcalorimetric (ITC) measurements of Pch-GlmA enzyme kinetics

Prior to enzymatic activity measurements, the protein was annealed by incubating it at 60 °C for at least 5 min. Such an annealing step was necessary to obtain enzymatic activity from another enzyme in the chitinolytic pathway of *P. chitonophagus*, namely *N,N*-diacetylchitobiose deacetylase (*Pch*-Dac) (Biniek-Antosiak et al., 2022).

MicroCal PEAQ-ITC (Malvern) and iTC200 (Malvern) calorimeters were used in the multiple-injection mode (Wang et al., 2020). The enthalpy of total substrate-to-product conversion (H_{app} i.e., the total molar reaction enthalpy) was examined by injecting small aliquots of substrate (2 μL of 1–50 mM solutions of GlcNAc-GlcN, GlcN-GlcNAc, $(GlcNAc)_2$ or $(GlcN)_2$) (purchased from Megazyme by Neogen) from the syringe into the reaction cell containing the enzyme at 2–13 μM. Injections were separated by sufficiently long intervals to allow the baseline to return to its initial differential power value, which theoretically indicates complete substrate conversion.

Blank experiments were performed to measure the heat of substrate dilution by injecting the same substrate solution into buffer. After peak integration using the Microcal PEAQ-ITC Analysis Software (Malvern), the values were averaged to obtain H_{app}.

Experiments were conducted in a range of buffer systems, including MES and HEPES, as well as SPG (glycine, sodium phosphate monohydrate and succinic acid; pH 4.0–10.0). For SPG, conditions were tested both in the presence (5 mM DTT, 1–5 mM TCEP, or 5 mM 2-mercaptoethanol) and absence of reducing agents, with pH values from 5.5 to 9.0. Temperatures from 25 to 75 °C were examined. The stirring speed was

set to 650–700 rpm, and the differential power 10 μcal/s.

4.7. NMR spectroscopy

Experiments aimed at detecting *Pch*-GlmA activity and identifying possible substrate-product transformation were performed using NMR spectroscopy. Initial measurements were carried out on samples containing *Pch*-GlmA with the appropriate ligands, which had been incubated for 1 h at 60 °C, and subsequently on samples incubated under the same conditions at 90 °C.

1H and ^{13}C NMR experiments were conducted at 25 °C in HEPES buffer containing 10% D_2O on a Bruker Avance III 700 MHz spectrometer equipped with a 5 mm QCI-P CryoProbe™. Chemical shifts were referenced to internal 4,4-dimethyl-4-silapentane-1-sulfonic acid (DSS). Analyte samples for NMR were prepared at a concentration of 50 mM in HEPES buffer (pH 7.5) with 10% D_2O (*w/w*). The water signal was suppressed using the excitation-sculpting with gradients method (Hwang and Shaka, 1995). The ^{1}H NMR spectra were acquired with 64 k data points over a spectral width of 13 ppm. A relaxation delay of 1 s was applied, and 64 scans were accumulated for each spectrum. Each acquisition required 3.60 s. The ^{13}C NMR spectra were recorded using a one-dimensional sequence with power-gated decoupling and 30° flip angle. The number of data points and spectral width were set to 64 k and 210 ppm, respectively.

Signal assignments for ^{1}H and ^{13}C nuclei were obtained using ^{1}H – ^{1}H COSY and ^{1}H – ^{13}C HSQC experiments. All two-dimensional homo- and heteronuclear correlation experiments were performed using standard parameter sets. Spectra were processed, analyzed and prepared using Bruker TopSpin 4.5 software.

Abbreviations

Pch-GlmA	*exo*-β-D-glucosaminidase from *Pyrococcus chitonophagus*
GlcN	D-glucosamine
GlcNAc	*N*-acetyl-D-glucosamine
GlcNAc-GlcN	1,4-β-D-*N*-acetylglucosaminyl-D-glucosamine
GlcN-GlcNAc	1,4-β-D-glucosaminyl-D-*N*-acetylglucosamine
GlcNAc-GlcNAc	1,4-β-D-*N*-acetylglucosaminyl-D-*N*-acetylglucosamine
GlcN-GlcN	1,4-β-D-glucosaminyl-D-glucosamine
DSC	Differential Scanning Calorimetry
NanoDSF	Nano Differential Scanning Fluorimetry
ITC	Isothermal Titration Calorimetry
DSS	4,4-dimethyl-4-silapentane-1-sulfonic acid; standard used in NMR

CRediT authorship contribution statement

Katarzyna Biniek-Antosiak: Visualization, Validation, Investigation, Conceptualization. **Daniel Baranowski:** Writing – original draft, Validation, Investigation, Data curation, Conceptualization. **Joanna Śliwiak:** Writing – original draft, Validation, Investigation, Data curation, Conceptualization. **Mariusz Milik:** Validation, Methodology, Investigation. **Magdalena Bejger:** Validation, Investigation. **Wojciech Rypniewski:** Writing – original draft, Visualization, Validation, Supervision, Project administration, Funding acquisition, Data curation, Conceptualization.

Declaration of competing interest

The authors declare that they have no known competing financial interests or personal relationships that could have appeared to influence the work reported in this paper.

Acknowledgments

The research was co-funded by the National Science Centre, Poland (UMO-2017/27/B/NZ1/02201). We thank dr hab. Joanna Loch from Jagiellonian University for providing access to the Prometheus Panta instrument and software. This study was carried out using research infrastructure funded by the European Union in the framework of the Smart Growth Operational Programme, Measure 4.2, Grant No. POIR.04.02.00-00-D001/20, ATOMIN 2.0 – Center for materials research on ATOMic scale for the INnovative economy. We would like to thank Future Synthesis sp. z o.o. for support and reagents.

Appendix A. Supplementary data

Supplementary data to this article can be found online at https://doi.org/10.1016/j.jsb.2026.108327.

Data availability

Data will be made available on request.

References

Biniek-Antosiak, K., Bejger, M., Śliwiak, J., Baranowski, D., Mohammed, A.S.A., Svergun, D.I., Rypniewski, W., 2022. Structural, thermodynamic and enzymatic characterization of N,N-diacetylchitobiose deacetylase from pyrococcus chitonophagus. Int. J. Mol. Sci. 23, 15736. https://doi.org/10.3390/ijms232415736.

Cherinka, B., Andrews, B.H., Sánchez-Gallego, J., Brownstein, J., Argudo-Fernández, M., Blanton, M., Bundy, K., Jones, A., Masters, K., Law, D.R., Rowlands, K., Weijmans, A.-M., Westfall, K., Yan, R., 2019. Marvin: a tool kit for streamlined access and visualization of the SDSS-IV MaNGA data set. AJ 158, 74. https://doi.org/10.3847/1538-3881/ab2634.

Cianci, M., Bourenkov, G., Pompidor, G., Karpics, I., Kallio, J., Bento, I., Roessle, M., Cipriani, F., Fiedler, S., Schneider, T.R., IUCr, 2017. P13, the EMBL macromolecular crystallography beamline at the low-emittance PETRA III ring for high- and low-energy phasing with variable beam focusing. urn:issn:1600–5775 J. Synchrotron Radiat. 24, 323–332. https://doi.org/10.1107/S1600577516016465.

Emsley, P., Lohkamp, B., Scott, W.G., Cowtan, K., 2010. Features and development of Coot. Acta Crystallogr. D Biol. Crystallogr. 66, 486–501. https://doi.org/10.1107/S0907444910007493.

Gooday, G.W., 1990. The ecology of chitin degradation. In: Marshall, K.C. (Ed.), Advances in Microbial Ecology. Springer US, Boston, MA, pp. 387–430. https://doi.org/10.1007/978-1-4684-7612-5_10.

Gu, Z., Rao, M.K., Forsyth, W.R., Finke, J.M., Matthews, C.R., 2007. Structural analysis of kinetic folding intermediates for a TIM barrel protein, indole-3-glycerol phosphate synthase, by hydrogen exchange mass spectrometry and Gō-model simulation. J. Mol. Biol. 374, 528–546. https://doi.org/10.1016/j.jmb.2007.09.024.

Huber, R., Stöhr, J., Hohenhaus, S., Rachel, R., Burggraf, S., Jannasch, H.W., Stetter, K. O., 1995. *Thermococcus chitonophagus* sp. nov., a novel, chitin-degrading, hyperthermophilic archaeum from a deep-sea hydrothermal vent environment. Arch. Microbiol. 164 (4), 255–264. https://doi.org/10.1007/BF02529959.

Hwang, T.L., Shaka, A.J., 1995. Water suppression that works. Excitation sculpting using arbitrary wave-forms and pulsed-field gradients. J. Magn. Reson. A 112, 275–279. https://doi.org/10.1006/jmra.1995.1047.

Jakalian, A., Bush, B.L., Jack, D.B., Bayly, C.I., 2000. Fast, efficient generation of high-quality atomic charges. AM1-BCC model: I method. J. Comput. Chem. 21, 132–146. https://doi.org/10.1002/(SICI)1096-987X(20000130)21:2%253C132::AID-JCC5%253E3.0.CO;2-P.

Kabsch, W., 2010. XDS. Acta Crystallogr. D Biol. Crystallogr. 66, 125. https://doi.org/10.1107/S0907444909047337.

Krissinel, E., Henrick, K., 2007. Inference of macromolecular assemblies from crystalline state. J. Mol. Biol. 372, 774–797. https://doi.org/10.1016/j.jmb.2007.05.022.

McCoy, A.J., Grosse-Kunstleve, R.W., Adams, P.D., Winn, M.D., Storoni, L.C., Read, R.J., 2007. Phaser crystallographic software. J. Appl. Cryst. 40, 658–674. https://doi.org/10.1107/S0021889807021206.

Mine, S., Watanabe, M., 2019. Structural insights into the molecular evolution of the archaeal Exo-β-d-Glucosaminidase. Int. J. Mol. Sci. 20, 2460. https://doi.org/10.3390/ijms20102460.

Mine, S., Niiyama, M., Hashimoto, W., Ikegami, T., Koma, D., Ohmoto, T., Fukuda, Y., Inoue, T., Abe, Y., Ueda, T., Morita, J., Uegaki, K., Nakamura, T., 2014. Expression from engineered *Escherichia coli* chromosome and crystallographic study of archaeal N,N′-diacetylchitobiose deacetylase. FEBS J. 281, 2584–2596. https://doi.org/10.1111/FEBS.12805.

Mine, S., Watanabe, M., Kamachi, S., Abe, Y., Ueda, T., 2017. The structure of an archaeal α-Glucosaminidase provides insight into glycoside hydrolase evolution. J. Biol. Chem. 292, 4996–5006. https://doi.org/10.1074/JBC.M116.766535.

Murshudov, G.N., Skubák, P., Lebedev, A.A., Pannu, N.S., Steiner, R.A., Nicholls, R.A., Winn, M.D., Long, F., Vagin, A.A., 2011. REFMAC5 for the refinement of macromolecular crystal structures. Acta Crystallogr. D Biol. Crystallogr. 67, 355. https://doi.org/10.1107/S0907444911001314.

Nakamura, T., Niiyama, M., Hashimoto, W., Ida, K., Abe, M., Morita, J., Uegaki, K., IUCr, 2015. Multiple crystal forms of N,N′-diacetylchitobiose deacetylase from *Pyrococcus*

furiosus. Acta Crystallogr. F Struct. Biol. Commun. 71, 657–662. https://doi.org/10.1107/S2053230X15005695.

Nakamura, T., Yonezawa, Y., Tsuchiya, Y., Niiyama, M., Ida, K., Oshima, M., Morita, J., Uegaki, K., 2016. Substrate recognition of N,N'-diacetylchitobiose deacetylase from *Pyrococcus horikoshii*. J. Struct. Biol. 195, 286–293. https://doi.org/10.1016/J.JSB.2016.07.015.

Pettersen, E.F., Goddard, T.D., Huang, C.C., Couch, G.S., Greenblatt, D.M., Meng, E.C., Ferrin, T.E., 2004. UCSF Chimera–a visualization system for exploratory research and analysis. J. Comput. Chem. 25, 1605–1612. https://doi.org/10.1002/jcc.20084.

Tanaka, T., Fukui, T., Atomi, H., Imanaka, T., 2003. Characterization of an Exo-β-d-Glucosaminidase involved in a novel Chitinolytic pathway from the Hyperthermophilic archaeon Thermococcus kodakaraensis KOD1. J. Bacteriol. 185, 5175–5181. https://doi.org/10.1128/jb.185.17.5175-5181.2003.

Tanaka, T., Fukui, T., Fujiwara, S., Atomi, H., Imanaka, T., 2004. Concerted action of Diacetylchitobiose deacetylase and Exo-β-D-glucosaminidase in a novel Chitinolytic pathway in the Hyperthermophilic archaeon *Thermococcus kodakaraensis* KOD1*. J. Biol. Chem. 279, 30021–30027. https://doi.org/10.1074/jbc.M314187200.

Tian, C., Kasavajhala, K., Belfon, K.A.A., Raguette, L., Huang, H., Migues, A.N., Bickel, J., Wang, Y., Pincay, J., Wu, Q., Simmerling, C., 2020. ff19SB: amino-acid-specific protein backbone parameters trained against quantum mechanics energy surfaces in solution. J. Chem. Theory Comput. 16, 528–552. https://doi.org/10.1021/acs.jctc.9b00591.

Wang, Y., Wang, G., Moitessier, N., Mittermaier, A.K., 2020. Enzyme kinetics by isothermal titration calorimetry: allostery, inhibition, and dynamics. Front. Mol. Biosci. 7. https://doi.org/10.3389/FMOLB.2020.583826.

Winn, M.D., Ballard, C.C., Cowtan, K.D., Dodson, E.J., Emsley, P., Evans, P.R., Keegan, R.M., Krissinel, E.B., Leslie, A.G.W., McCoy, A., McNicholas, S.J., Murshudov, G.N., Pannu, N.S., Potterton, E.A., Powell, H.R., Read, R.J., Vagin, A., Wilson, K.S., 2011. Overview of the CCP4 suite and current developments. Acta Crystallogr. D Biol. Crystallogr. 67, 235–242. https://doi.org/10.1107/S0907444910045749.